Pacific Northwest
NATIONAL LABORATORY

PNNL- 38386

Computational investigation of thermophysical and structural properties of molten $NaCl-PuCl_3-AmCl_3$

September 2025

Manh-Thuong Nguyen

U.S. DEPARTMENT of ENERGY

Prepared for the U.S. Department of Energy
under Contract DE-AC05-76RL01830

PACIFIC NORTHWEST NATIONAL LABORATORY
operated by
BATTELLE
for the
UNITED STATES DEPARTMENT OF ENERGY
under Contract DE-AC05-76RL01830

Printed in the United States of America

Available to DOE and DOE contractors from
the Office of Scientific and Technical Information,
P.O. Box 62, Oak Ridge, TN 37831-0062
www.osti.gov
ph: (865) 576-8401
fox: (865) 576-5728
email: reports@osti.gov

Available to the public from the National Technical Information Service
5301 Shawnee Rd., Alexandria, VA 22312
ph: (800) 553-NTIS (6847)
or (703) 605-6000
email: info@ntis.gov
Online ordering: http://www.ntis.gov

PNNL- 38386

Computational investigation of thermophysical and structural properties of molten NaCl-$PuCl_3$-$AmCl_3$

September 2025

Manh-Thuong Nguyen

Prepared for
the U.S. Department of Energy
under Contract DE-AC05-76RL01830

Pacific Northwest National Laboratory
Richland, Washington 99354

Summary

This work is aimed at providing thermophysical properties of molten NaCl-$PuCl_3$-$AmCl_3$, which is highly relevant to molten salt reactors. First, ab initio molecular dynamics (AIMD) simulations were conducted to generate high-fidelity reference datasets, on which a machine learning potential was trained. This potential, designed to preserve AIMD-level accuracy while allowing for extensive sampling, was then used in molecular dynamics simulations to calculate various thermophysical properties of the system. Specifically, the density, thermal expansion coefficient, heat capacity, viscosity, and thermal conductivity were evaluated. Moreover, temperature-dependent relationships for the density, thermal expansion coefficient, and viscosity were established. In addition to thermophysical calculations, structural properties of the mixture were also analyzed.

Acknowledgments

This work was supported by the Molten Salt Reactor Program, work package number AT-25PN070506 “Thermophysical Property Database Development-Modeling −PNNL”.

Acronyms and Abbreviations

AIMD	Ab initio molecular dynamics
Cp	Constant pressure heat capacity
DFT	Density functional theory
GPW	Gaussian plane wave
H	Enthalpy
LAMMPS	Large-scale Atomic/Molecular Massively Parallel Simulator
MLIP	Machine learning interatomic potential
MS	Molten salt
MSR	Molten salt reactor
RMSEs	Root mean square errors

Contents

Figures

Tables

1.0 Introduction

In molten salt reactors (MSRs), minor actinides are closely related to advanced fuel cycles, contributing to both energy production and long-term waste reduction. Americium trichloride ($AmCl_3$), in particular, is highly relevant to chloride-based MSR systems. Significant progress has been made in advancing the fundamental understanding of $AmCl_3$ through multiple research avenues. At the molecular level, electronic structure theory has been used to investigate its gas-phase complexes and solid-state properties, providing insights into bonding, electronic, and structural behavior (Vetere et al. 2004; Li et al. 2023). Experimentally, the synthesis of $AmCl_3$ has received increasing attention, with several alternative strategies being employed (Hayashi et al. 2008; Kersten et al. 2022; Chevreux et al. 2024). In parallel, the electrochemical behavior of $AmCl_3$-bearing molten salts (MSs) has been investigated (Filatov et al. 2023; Serp et al. 2006), highlighting its potential role in actinide separation, redox control, and MSR applications. All together, these studies underscore the importance of $AmCl_3$ across theory, synthesis, and applied electrochemistry, while also pointing to the need for further investigation of its thermophysical properties in technologically relevant environments. Thus far, the eutectic composition of the binary NaCl-$AmCl_3$ system has been predicted to at 40-45 mol% $AmCl_3$. (Toni Y Karlsson and Pinto 2024) Very limited thermophysical property data for $AmCl_3$-based MSs are currently available in the literature. The lack of fundamental data will pose barriers to reactor safety assessments and fuel cycle optimization. Addressing this gap is essential for enabling the reliable deployment of chloride-based MSR technologies.

In this work, by leveraging recent advances in machine learning interatomic potentials (MLIPs), we investigated key thermophysical properties of a NaCl-$PuCl_3$-$AmCl_3$ ternary MS with approximately 31 mol% $PuCl_3$ and 14 mol% $AmCl_3$, including the liquid density, thermal expansion, heat capacity, viscosity, and thermal conductivity. The use of machine learning-based potentials allows for accurate, large-scale molecular dynamics simulations at a fraction of the computational cost of traditional ab initio methods, thereby enabling reliable predictions of temperature-dependent trends. This approach not only provides quantitative estimates of fundamental properties but also helps gain new insights into the underlying atomic-scale mechanisms governing thermal, transport and structural behavior in complex molten systems.

2.0 Methods

As demonstrated in our previous works as well as in the literature, MLIPs can significantly accelerate atomistic modeling of MS systems (Nguyen et al. 2023; Nguyen et al. 2025; Xu et al. 2023). Studies of actinide-bearing MSs stand to benefit substantially from the use of MLIPs. High-accuracy methods based on electronic structure theory, such as ab initio molecular dynamics, provide critical insight but are computationally prohibitive for the large-scale simulations required to capture transport properties complex liquids. MLIPs, by contrast, can reproduce ab initio accuracy at a fraction of the computational cost, enabling simulations that are both extensive and predictive, making them especially valuable for actinide-bearing systems, where experimental data are scarce and direct measurements are often limited.

To create a MLIP for the NaCl-$PuCl_3$-$AmCl_3$ system, the following workflow was employed. We began by conducting AIMD simulations to generate reference datasets, including atomic coordinates, energies, and forces, for the system. These datasets were then used to train a MLIP capable of reproducing the accuracy of AIMD. Finally, the trained potential was applied in large-scale molecular dynamics simulations, enabling the efficient calculation of key thermophysical properties of the mixture.

2.1 Ab initio molecular dynamics

AIMD simulations were carried out using CP2K (Kühne et al. 2020). The energy was calculated with spin-polarized revPBE-vdW (Zhang and Yang 1998; Dion et al. 2004) density functional calculations. The Gaussian and Plane-wave (GPW) hybrid basis set scheme (Lippert, Hutter, and Parrinello 1997) was employed, with the double-zeta valence polarized (DZVP) (Doudin et al. 2019; Lu et al. 2021) Gaussian basis sets and a plane wave cutoff of 600 Ry. The GTH pseudopotentials (Lu et al. 2021; Goedecker, Teter, and Hutter 1996) were used with the number of valence electrons being 1 for Na, 16 (Pu), 17 (Am) and 7 (Cl). The accuracy of this density functional theory (DFT) approach is demonstrated below for solid state systems. The initial structure and density of the system at each temperature were prepared using molecular dynamics based on the polarized ionic model (Salanne and Madden 2011). AIMD simulations were then carried out with isothermal-isobaric ensemble (NPT) in which the pressure (1 bar) and temperature were controlled with the Nose-Hoover chain barostat/thermostat (Martyna, Klein, and Tuckerman 1992). A 2-fs time step was used.

2.2 Machine learning interatomic potentials

In this work we employed the DeepMD potential model (Zeng et al. 2023) implemented in the DeePMD-kit (Zeng et al. 2023) to train MLIPs. In this approach, the energy of the system is given by

$$E = \sum_i E_i = \sum_i N(D_i(\boldsymbol{R}_i))$$

where E_i is the local atomic energy determined by atom *i* and its neighbors within a cutoff R_c, the descriptor D_i is the feature matrix encoding the surrounding environment and is fed to a deep neural network N which returns the energy E_i. $\boldsymbol{R_i}$ is the set coordinates of all atoms in the environment, $\boldsymbol{R}_i = \{\boldsymbol{r}_{ij} \equiv \boldsymbol{r}_i - \boldsymbol{r}_j\}$.

The network is trained by minimizing the loss function

$$\mathcal{L} = p_E|\Delta E|^2 + \frac{p_f}{3N}\sum_i |\Delta F_i|^2$$

in which ΔE and ΔF are the deviation of the potential energy and atomic forces between the reference AIMD and predicted data, respectively; and p_E and p_f are tunable pre-factors.

Here we used a radial cutoff and a smooth cutoff of 7.0 and 6.5 Å, respectively. The pre-factor p_E was set to increase from 0.02 to 1 and p_f was set to decrease from 1000 to 1. We employed 20,40,80} embedding and 250,250,250} fitting network.

From 46000 AIMD frames, 37000 frames were randomly chosen to create a training set, similarly, 4500 frames for a validation set and 4500 frames for a test set.

2.3 Molecular dynamics based on machine learning interatomic potentials

Machine learning interatomic potential molecular dynamics (MLIPs) were conducted using Large-scale Atomic/Molecular Massively Parallel Simulator (LAMMPS) (Thompson et al. 2022). To calculate the liquid density we employed the NPT ensemble in which the pressure P and temperature T were maintained with Nosé–Hoover barostat/thermostat (Evans and Holian 1985). The time step was set at 1 fs. Viscosity calculations were performed using the NVT ensemble where the temperature was controlled with the Nosé–Hoover thermostat.

2.4 Atomic systems

Here we employed cubic boxes consisting of 110 Cl, 32 Na, 18 Pu, and 8 Am atoms, Figure 1, corresponding to the composition of approximately 55 mol% NaCl, 31 mol% $PuCl_3$, and 14 mol%

$AmCl_3$. This is equivalent to adding about 14 mol% $AmCl_3$ to the eutectic binary system of NaCl and $PuCl_3$.

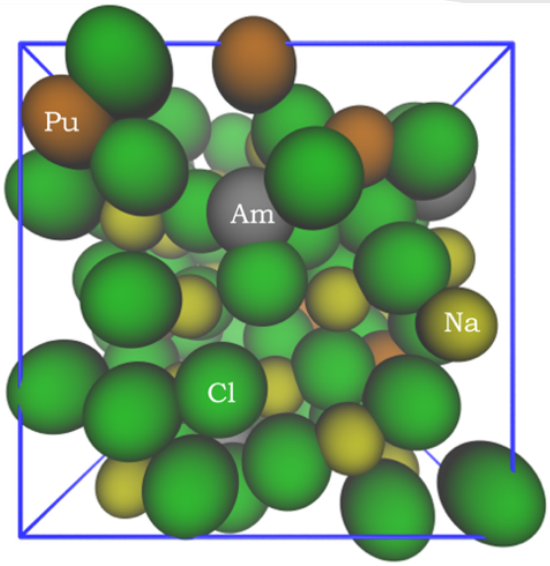

Figure 1. A simulation box with Cl in green, Na in yellow, Pu in orange, and Am in grey.

3.0 Results

3.1 Solid state systems

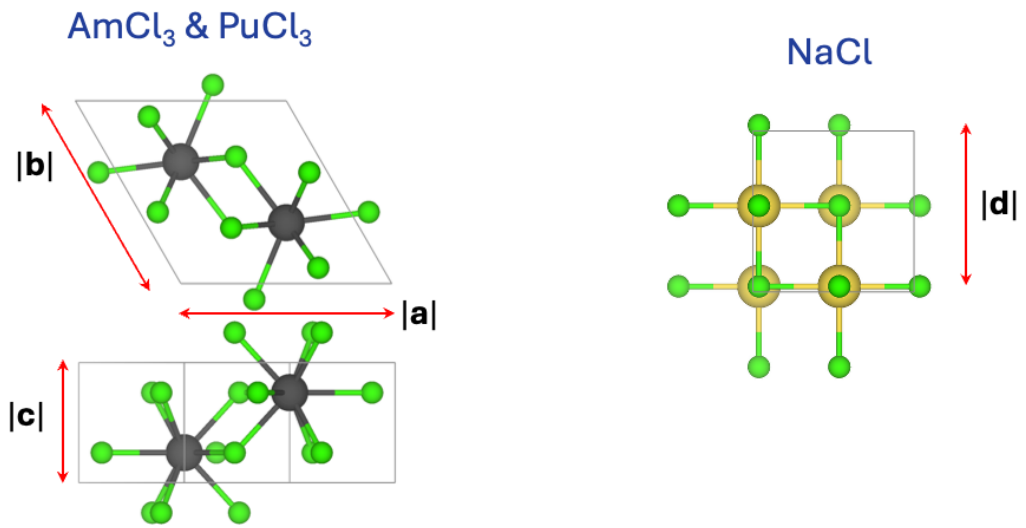

Figure 2. Solid state structures of three solids with chlorine in green and metal in grey/orange.

To test the accuracy of the DFT method in use, we first calculated the lattice constants of three solids: NaCl, $PuCl_3$, and $AmCl_3$. While solid $AmCl_3$ and $PuCl_3$ adopt the P63/m, NaCl has the Fm-3m space group, Figure 2. A supercell equivalent to 2×2×4 and 3×3×3 primitive unit cells was used for $AmCl_3$/$PuCl_3$ and NaCl, respectively. Only the *Gamma* point was used to sample the Brillouin zone in DFT calculations. In the actinide chloride systems, the ferromagnetic spin configuration appeared to be slightly more stable than the antiferromagnetic one. Table 1 shows that these calculated parameters agree well with experimental data, indicating the accuracy of the DFT method employed in this work.

Table 1. Calculated and experimental lattice constants and errors. Experimental data for actinide chlorides (Asprey, Keenan, and Kruse 1965; Burns, Peterson, and Stevenson 1975) and sodium chloride (Froyen and Cohen 1986) taken the literature.

	$AmCl_3$			$PuCl_3$			NaCl		
	Cal.	Exp.	Err.(%)	Cal.	Exp.	Err.(%)	Cal.	Exp.	Err.(%)
|a|=|b| (Å)	7.337	7.390	0.7	7.330	7.394	0.8			
|c| (Å)	4.234	4.234	~0.0	4.296	4.234	1.3			
|d| (Å)							5.665	5.640	0.4

3.2 Machine learning interatomic potential training

The root mean square errors (RMSEs) for different data sets, shown in Figure 4 and Table 2, provide a quantitative measure of the accuracy of the trained interatomic potential. Compared to the AIMD reference data sets, the observed deviations are small: the energy differences are about 1 meV per atom, while the force differences are approximately 60 meV/Å. These values are well within the range typically considered acceptable, demonstrating that the trained interatomic potential can reliably reproduce AIMD-level accuracy.

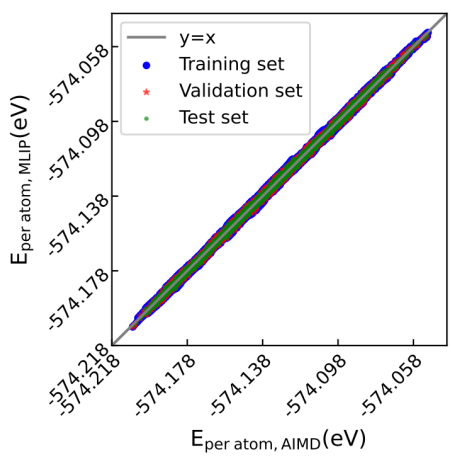

Figure 3. Potential energy calculated using the trained MLIP for different data sets versus AIMD data.

Table 2. Error of the energy (meV/atom) and force (meV/ Å) of the MLIP vs AIMD for different datasets

	Training set	Validation set	Test set
Energy RMSE	1.05	1.08	1.06
Force RMSE	59.5	59.6	59.6

3.3 Density

The density was calculated as

$$\rho = \frac{m}{V}$$

with m being the total atomic mass and *V* being the equilibrium volume of the simulation box. Since the mass *m* is independent of temperature, whereas the volume *V* changes with temperature, our task reduces to determining *V* at given temperatures. This was accomplished by using the PNT ensemble as mentioned in the method section. Figure 4 shows the variation of liquid density as a function of temperature, demonstrating the expected trend of decreasing density with rising temperature. The numerical data were fitted to a linear relationship, resulting in the equation $\rho = 4.54 - 9.4 \times 10^4 \times T,\ R = 0.999$.

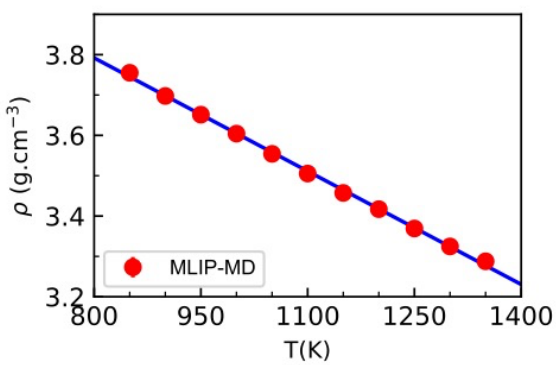

Figure 4. Temperature dependence of density.

3.4 Thermal expansion coefficient

The decrease of the density with temperature reflects the thermal expansion of the system. The thermal expansion was evaluated as

$$\beta = \frac{1}{V}\left(\frac{\partial V}{\partial T}\right)_p = -\frac{1}{\rho}\left(\frac{\partial \rho}{\partial T}\right)_p$$

which was calculated directly from the density data. Figure 5 shows that the thermal expansion is relatively small in magnitude; nevertheless, it increases progressively as the temperature

rises. This is indicative of enhanced structural flexibility at higher temperatures. Fitting the numerical data to the linear equation leads to $\beta = 1.5\ 10^{-4} + 6\ \times 10^{-8}\ T$

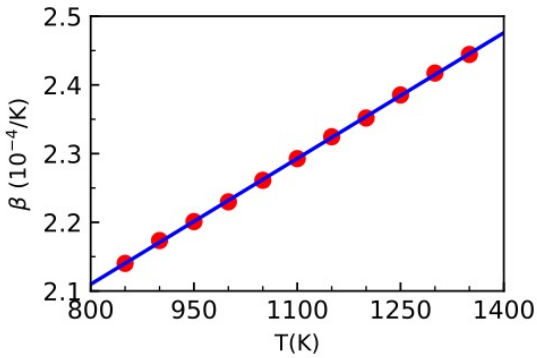

Figure 5. Thermal expansion coefficient as a function of temperature.

3.5 Constant pressure specific heat capacity Cp

We evaluated constant pressure specific heat capacity C_p by using the variation of the enthalpy with temperature:

$$C_p = \left(\frac{\partial H}{\partial T}\right)_p \approx \frac{\Delta H}{\Delta T}$$

Figure 6 shows that the enthalpy varies linearly with temperature over the examined range of temperature. It is thus straightforward to evaluate the specific heat which amounts to 0.55 J/gK which is slightly lower than measured values (~0.6 J/gK) of the binary NaCl-$PuCl_3$ with 36 mol% $PuCl_3$ (Toni Y. Karlsson et al. 2023), which has a lower actinide content.

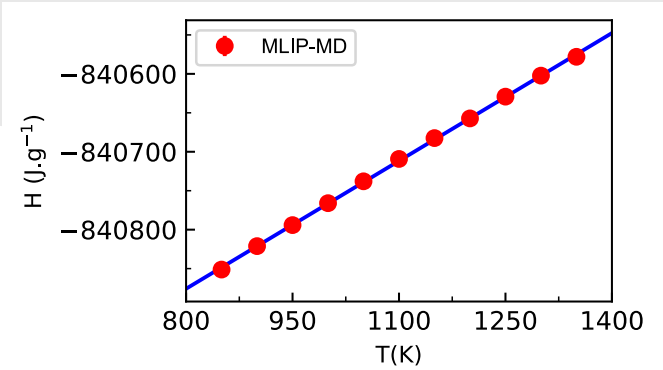

Figure 6. Temperature dependence of enthalpy.

3.6 Viscosity

We calculated the viscosity by using the Green Kubo approach

$$\eta = \frac{V}{k_B T} \int_0^t \langle P_{xy}(0) P_{xy}(t') \rangle dt'$$

in which V denotes the volume of the simulation box, k_B is the Boltzmann constant, T is the temperature, P_{xy} is an off-diagonal component of pressure tensor, and the angle brackets ⟨...⟩ indicate an ensemble average. A major challenge in this calculation is the poor convergence of η as a function of time. To mitigate this, several independent simulations were carried out at each temperature, and their results were averaged, as demonstrated in Figure 7(a).

Figure 7(b) shows the viscosity decreases rapidly with the temperature. Fitting the numerical data to an Arrhenius-type equation a functional relationship between η and T

$$\eta = A \times e^{B/k_B T}$$

we obtained 0.0044 mPa.s and 0.383 eV for parameters A and B, respectively.

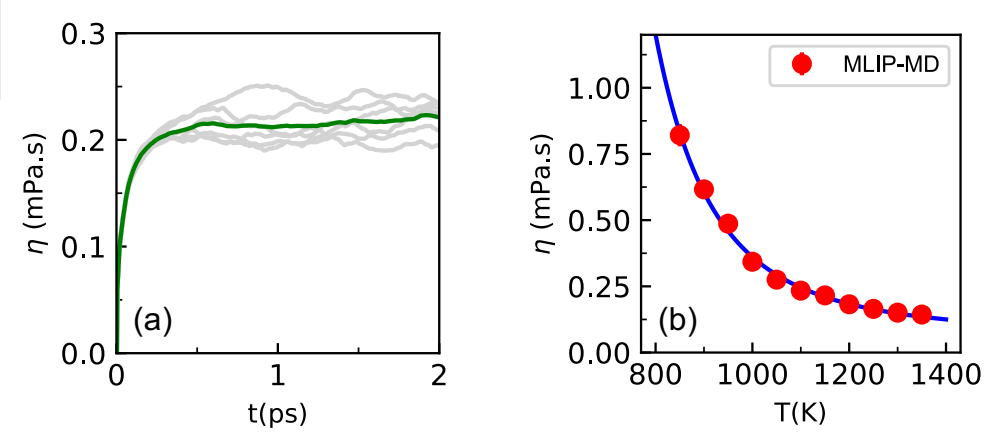

Figure 7. Viscosity as a function of time from several independent simulations (grey) and the averaged data (green) at 1150 K, (b) Temperature dependence of viscosity.

3.7 Thermal conductivity

We used the variant of Muller-Plathe reverse perturbation method (Plimpton 2014) to evaluate the thermal conductivity

$$\kappa = \frac{\Delta Q}{2\,A\,\Delta t} \times \frac{1}{\Delta T/\Delta \mathrm{z}}$$

in which ΔQ denotes the amount of heat added to a "hot" region and removed from a "cold" region along the z direction (Figure 8(a)), A is the cross-sectional area of the simulation box in the xy-plane, $1/\Delta t$ is the frequency at which ΔQ is added or removed; and $\Delta T/\Delta \mathrm{z}$ represents the temperature gradient along the direction from the hot to the cold regions. In our thermal conductivity calculations, the cubic simulation box described above was extended by replicating it three times along the z-direction. Figure 8(b) shows linear changes of the temperature between the hot and cold regions which allow for evaluation of the gradient.

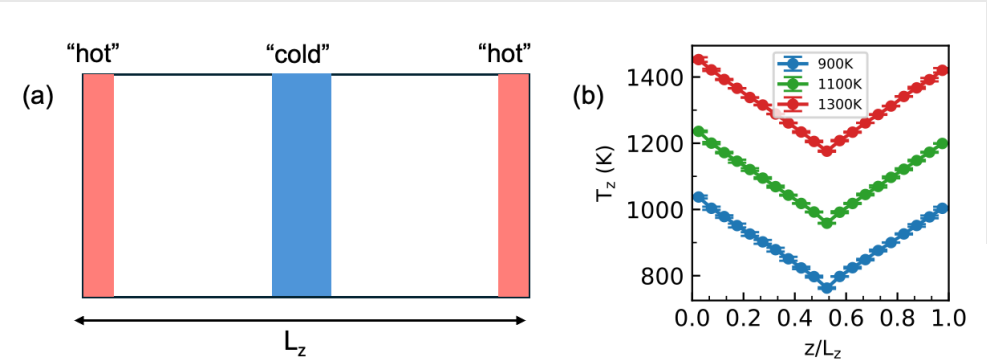

Figure 8. (a) Schematic illustration of the "hot" and "cold" regions along the z direction under periodic boundary conditions, (b) The variation of temperature along the z direction, (c) Theral conductivity at different temperatures.

Figure 9 shows that (i) the thermal conductivity of the system is in the 0.2-0.3 (W cm^{-1} K^{-1}) range and (ii) it decreases with the temperature. The thermal conductivity of this system is lower than that of pure NaCl, which has been measured to be 0.4-0.5 (W cm^{-1} K^{-1}) (Harada et al. 1992). Understandably, adding more heavy atoms would reduce vibrational frequencies in the system, lowering the thermal conductivity.

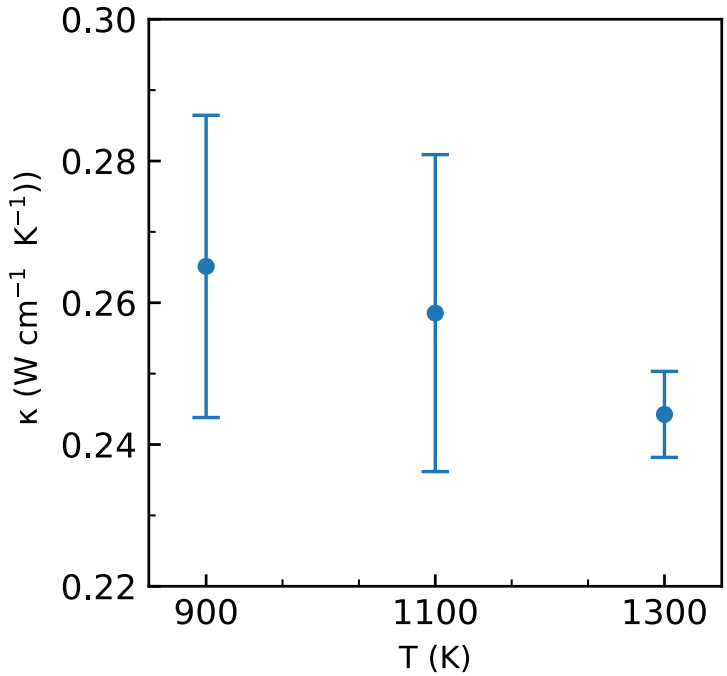

Figure 9. Thermal conductivity at different temperatures.

3.8 Structural properties

To understand how metal ions interact with the counterion Cl^-, we calculated the radial distribution functions (RDFs), g(r), for cation–anion pairs in the system at 1200 K (Figure 10). The positions of the first peaks in g(r) indicate that the Am–Cl and Pu–Cl bond distances are almost the same (2.73 Å), and both are slightly larger than the Na–Cl bond distance (2.71 Å). The RDFs also suggest that the Na–Cl interaction is weaker than the interactions of Am–Cl and Pu–Cl. This is in part due to the charge difference of the metal ions. The Cl^- coordination number (i.e., the ensemble-averaged number of chloride ions in the first coordination shell of each cation is 7.0 for Pu, 7.1 for Am, and 6.2 for Na.

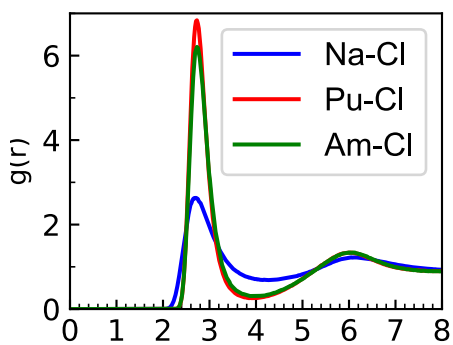

Figure 10. Radial distribution functions of cation-anion pairs.

4.0 Concluding remarks

Using molecular dynamics, we calculated the density, thermal expansion, specific heat capacity, viscosity, and thermal conductivity of a ternary system of NaCl-$PuCl_3$-$AmCl_3$ with approximately 31 mol% $PuCl_3$ and 14 mol% $AmCl_3$. Ab initio molecular dynamics was first employed to generate datasets used for training an accurate machine learning interatomic potential that allowed for extensive sampling of the system. Linear equations for the temperature dependence of the density and thermal expansion were determined. The viscosity was found to decrease exponentially with increasing temperature. Next, thermal conductivity was calculated, showing a decline with temperature. Structural properties were finally calculated to understand fundamental interactions between ions. This work provides the first evaluation of the thermophysical properties of an important molten mixture, $AmCl_3$-$PuCl_3$-NaCl, which is relevant to fast spectrum molten salt reactors. Finally, we will be able to compare calculated data in this report with experimental data being determined at Idaho National Laboratory, and this will be presented in a peer-reviewed journal article planned for FY 2026.

5.0 References

Asprey, LB, TK Keenan, and FH Kruse. 1965. "Crystal structures of the trifluorides, trichlorides, tribromides, and triiodides of americium and curium." *Inorganic Chemistry* 4 (7): 985-986.

Burns, John H, JR Peterson, and JN Stevenson. 1975. "Crystallographic studies of some transuranic trihalides: 239PuCl3, 244CmBr3, 249BkBr3 and 249CfBr3." *Journal of Inorganic and Nuclear Chemistry* 37 (3): 743-749.

Chevreux, P, M Duchateau, G Serve, and M Pons. 2024. *Synthesis of Actinide Chlorides as Fuel for Fast Molten Salt Reactor.*

Dion, M., H. Rydberg, E. Schröder, D. C. Langreth, and B. I. Lundqvist. 2004. "Van der Waals Density Functional for General Geometries." *Physical Review Letters* 92 (24): 246401. https://doi.org/10.1103/PhysRevLett.92.246401. https://link.aps.org/doi/10.1103/PhysRevLett.92.246401.

Doudin, Nassar, Simuck F Yuk, Matthew D Marcinkowski, Manh-Thuong Nguyen, Jin-Cheng Liu, Yang Wang, Zbynek Novotny, Bruce D Kay, Jun Li, and Vassiliki-Alexandra Glezakou. 2019. "Understanding heterolytic H2 cleavage and water-assisted hydrogen spillover on Fe3O4 (001)-supported single palladium atoms." *ACS Catalysis* 9 (9): 7876-7887.

Evans, Denis J, and Brad Lee Holian. 1985. "The nose–hoover thermostat." *The Journal of chemical physics* 83 (8): 4069-4074.

Filatov, AA, MI Vlasov, AM Potapov, and Yu P Zaikov. 2023. "Possible electrochemical imitators for AmCl2 and CmCl3 in the Molten LiCl–KCl eutectic." *Russian Metallurgy (Metally)* 2023 (2): 244-247.

Froyen, Sverre, and Marvin L Cohen. 1986. "Structural properties of NaCl and KCl under pressure." *Journal of Physics C: Solid State Physics* 19 (15): 2623.

Goedecker, S., M. Teter, and J. Hutter. 1996. "Separable dual-space Gaussian pseudopotentials." *Physical Review B* 54 (3): 1703-1710. https://doi.org/DOI 10.1103/PhysRevB.54.1703. <Go to ISI>://WOS:A1996UZ86100053.

Harada, Makoto, Akihisa Shioi, Tsunetoshi Miura, and Shinsuke Okumi. 1992. "Thermal conductivities of molten alkali metal halides." *Industrial & engineering chemistry research* 31 (10): 2400-2407.

Hayashi, Hirokazu, Masahide Takano, Mitsuo Akabori, and Kazuo Minato. 2008. "Synthesis of americium trichloride by the reaction of americium nitride with cadmium chloride." *Journal of alloys and compounds* 456 (1-2): 243-246.

Karlsson, Toni Y, and Juliano Schorne Pinto. 2024. *Experimental Plan for Synthesis of an Americium and Plutonium Containing Salt.* Idaho National Laboratory (INL), Idaho Falls, ID (United States). INL/RPT-24-80052 Revision 0.

Karlsson, Toni Y., Scott C. Middlemas, Manh-Thuong Nguyen, Michael E. Woods, Kevin R. Tolman, Vassiliki-Alexandra Glezakou, Steven D. Herrmann, Juliano Schorne-Pinto, Ryan D. Johnson, Shawn E. Reddish, Stephen A. Warmann, and Patricia D. Paviet. 2023. "Synthesis and thermophysical property determination of NaCl-PuCl3 salts." *Journal of Molecular Liquids* 387: 122636. https://doi.org/https://doi.org/10.1016/j.molliq.2023.122636. https://www.sciencedirect.com/science/article/pii/S016773222301440X.

Kersten, Bethany, Krista Hawthorne, Mark Williamson, Rohan Akolkar, and Christine E Duval. 2022. "Synthesis of americium trichloride via chlorination of americium oxide using zirconium tetrachloride in LiCl–KCl molten salt." *Journal of Radioanalytical and Nuclear Chemistry* 331 (12): 4913-4918.

Kühne, Thomas D., Marcella Iannuzzi, Mauro Del Ben, Vladimir V. Rybkin, Patrick Seewald, Frederick Stein, Teodoro Laino, Rustam Z. Khaliullin, Ole Schütt, Florian Schiffmann, Dorothea Golze, Jan Wilhelm, Sergey Chulkov, Mohammad Hossein Bani-Hashemian, Valéry Weber, Urban Borštnik, Mathieu Taillefumier, Alice Shoshana Jakobovits, Alfio Lazzaro, Hans Pabst, Tiziano Müller, Robert Schade, Manuel Guidon, Samuel Andermatt, Nico Holmberg, Gregory K. Schenter, Anna Hehn, Augustin Bussy, Fabian Belleflamme, Gloria Tabacchi, Andreas Glöß, Michael Lass, Iain Bethune, Christopher J. Mundy, Christian Plessl, Matt Watkins, Joost VandeVondele, Matthias Krack, and Jürg Hutter. 2020. "CP2K: An electronic structure and molecular dynamics software package - Quickstep: Efficient and accurate electronic structure calculations." *The Journal of Chemical Physics* 152 (19). https://doi.org/10.1063/5.0007045.

Li, Ru‐song, Yu‐song He, Jin‐tao Wang, Zhi‐yong Liu, Yuan‐ming Wang, Ze‐lin Cao, and Zheng Xie. 2023. "Mixed 5 f configuration in americium trichloride: Dynamical mean‐field theory combined with density functional theory study." *International Journal of Quantum Chemistry* 123 (21): e27213.

Lippert, G., J. Hutter, and M. Parrinello. 1997. "A hybrid Gaussian and plane wave density functional scheme." *Molecular Physics* 92 (3): 477-487. https://doi.org/Doi 10.1080/00268979709482119. <Go to ISI>://WOS:A1997YC60700017.

Lu, Jun-Bo, David C. Cantu, Cong-Qiao Xu, Manh-Thuong Nguyen, Han-Shi Hu, Vassiliki-Alexandra Glezakou, Roger Rousseau, and Jun Li. 2021. "Norm-Conserving Pseudopotentials and Basis Sets to Explore Actinide Chemistry in Complex Environments." *Journal of Chemical Theory and Computation* 17 (6): 3360-3371. https://doi.org/10.1021/acs.jctc.1c00026. https://doi.org/10.1021/acs.jctc.1c00026.

Martyna, Glenn J, Michael L Klein, and Mark Tuckerman. 1992. "Nosé–Hoover chains: The canonical ensemble via continuous dynamics." *The Journal of chemical physics* 97 (4): 2635-2643.

Nguyen, Manh-Thuong, Vassiliki-Alexandra Glezakou, Roger Rousseau, and Patricia D Paviet. 2023. "Exploring NaCl-PuCl3 molten salts with machine learning interatomic potentials and graph theory." *Applied Materials Today* 35: 101951.

Nguyen, Manh-Thuong, Michael E. Woods, Juliano Schorne-Pinto, Nick H. Erfurth, Scott C. Middlemas, and Toni Karlsson. 2025. "Thermophysical Properties of NaCl–UCl3–PuCl3 Molten Salts: A Combined Computational and Experimental Study." *ACS Applied Energy Materials* 8 (10): 6482-6491. https://doi.org/10.1021/acsaem.5c00278. https://doi.org/10.1021/acsaem.5c00278.

Plimpton, Steven J. 2014. *Modeling thermal transport and viscosity with molecular dynamics.* Sandia National Lab.(SNL-NM), Albuquerque, NM (United States).

Salanne, Mathieu, and Paul A Madden. 2011. "Polarization effects in ionic solids and melts." *Molecular Physics* 109 (19): 2299-2315.

Serp, Jerome, Pierre Chamelot, Serge Fourcaudot, Rudy JM Konings, Rikard Malmbeck, Carole Pernel, Jean-Claude Poignet, Jean Rebizant, and J-P Glatz. 2006. "Electrochemical behaviour of americium ions in LiCl–KCl eutectic melt." *Electrochimica acta* 51 (19): 4024-4032.

Thompson, Aidan P, H Metin Aktulga, Richard Berger, Dan S Bolintineanu, W Michael Brown, Paul S Crozier, Pieter J In't Veld, Axel Kohlmeyer, Stan G Moore, and Trung Dac Nguyen. 2022. "LAMMPS-a flexible simulation tool for particle-based materials modeling at the atomic, meso, and continuum scales." *Computer Physics Communications* 271: 108171.

Vetere, Valentina, Björn O Roos, Pascale Maldivi, and Carlo Adamo. 2004. "A theoretical study of the bonding in trivalent americium complexes." *Chemical physics letters* 396 (4-6): 452-457.

Xu, Tingrui, Xuejiao Li, Yang Wang, and Zhongfeng Tang. 2023. "Development of deep potentials of molten MgCl2–NaCl and MgCl2–KCl salts driven by machine learning." *ACS Applied Materials & Interfaces* 15 (11): 14184-14195.

Zeng, Jinzhe, Duo Zhang, Denghui Lu, Pinghui Mo, Zeyu Li, Yixiao Chen, Marián Rynik, Li'ang Huang, Ziyao Li, and Shaochen Shi. 2023. "DeePMD-kit v2: A software package for deep potential models." *The Journal of Chemical Physics* 159 (5).

Zhang, Yingkai, and Weitao Yang. 1998. "Comment on ``Generalized Gradient Approximation Made Simple"." *Physical Review Letters* 80 (4): 890-890. https://doi.org/10.1103/PhysRevLett.80.890. https://link.aps.org/doi/10.1103/PhysRevLett.80.890.

PNNL- 38386

Pacific Northwest National Laboratory

902 Battelle Boulevard
P.O. Box 999
Richland, WA 99354

1-888-375-PNNL (7665)

www.pnnl.gov